RSC Advances

PAPER

View Article Online
View Journal | View Issue

Cite this: *RSC Adv.*, 2025, **15**, 35175

A DFT study on the base-catalyzed allylic rearrangement reaction of enol phosphate

Kangbo Wang,[a] Shuo Zhang,[a] Zhewei Li,[a] Wei Li,[a] Hexiang Qi,[a] Yanhui Tang[b] and Ming Lei *[a]

Enol phosphates are important intermediates for synthesizing bioactive molecules with neighboring C=C and C=O motifs, and their synthesis *via* the Perkow reaction is a highly attractive approach. The allyl rearrangement process involved in the Perkow reaction plays a key role in regulating the *Z*/*E* configuration of enol phosphate products. Herein, the mechanism of the base-catalyzed allylic rearrangement reaction of enol phosphates was investigated using density functional theory (DFT) methods. The calculated results of the NEt_3-catalyzed rearrangement reaction show that it undergoes two proton transfer steps and that the rate-determining step is the first proton transfer step with a free energy barrier of 20.7 kcal mol^{-1}. The modulation effect of different organic base catalysts (NEt_3, Py, $(i\text{-}Pr)_2NEt$, TBD, DBU, and MTBD) on this rearrangement is also discussed. It is found that it is difficult for weak bases such as pyridine to accept a proton from the substrate in the first proton transfer step and that strong bases such as *t*-BuOK do not perform well in the second proton transfer step. 1,8-Diazabicyclo[5.4.0]undecane-7-ene (DBU) is proposed as the optimum base to catalyze the allylic rearrangement reaction of enol phosphates, with a calculated energy barrier of 19.1 kcal mol^{-1} for the first proton transfer step. This study provides valuable guidance for screening efficient base catalysts for the synthesis of enol phosphates, and the approach could be applied to other base-catalyzed organic reactions.

Received 29th July 2025
Accepted 9th September 2025

DOI: 10.1039/d5ra05485k

rsc.li/rsc-advances

Introduction

The α,β-unsaturated ester group is an important motif in many organic intermediates and is commonly found in bioactive molecules exhibiting a broad range of functions in fields such as fine chemicals, pharmaceuticals, and polymers (see Scheme 1).[1] These motifs, featuring adjacent C=C and C=O double bonds, have opened up new reactivity and options for downstream functionalization.[2] Among various synthesis approaches, the strategy of directly converting saturated esters into the corresponding α,β-unsaturated counterparts *via* dehydrogenation is attractive and has been widely used in the synthesis of complex molecules.[3,4]

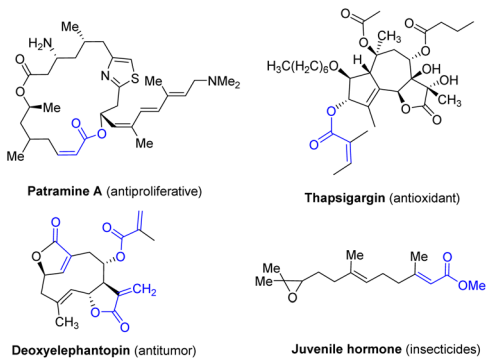

Scheme 1 Natural α,β-unsaturated ester motifs with biological activity.

However, most reactions using the dehydrogenation method rely on strong oxidizing reagents such as 2,3-dichloro-5,6-dicyano-1,4-benzoquinone (DDQ) or SeO_2 (see Scheme 2a).[5] In addition, the requirement for high temperature tends to result in low yields and poor selectivities, which limit their application. Another accessible synthetic strategy to obtain α,β-unsaturated esters is to synthesize the corresponding enol phosphate (EP) precursors first and then obtain α,β-unsaturated esters through Suzuki–Miyaura and Negishi reactions (Scheme 2b).[6–12] Nevertheless, the synthesis of phosphate esters remains an enormous challenge. Conventional organic synthesis strategies involving EPs include *in situ* metalation processes,[13] the Perkow reaction between phosphite and α-halogenones,[14,15] the phosphorylation of keto enolates and the hydrogen phosphorylation of alkynes (see Scheme 3a).[16,17] However, these synthetic

[a]*Beijing University of Chemical Technology, State Key Laboratory of Chemical Resource Engineering, Institute of Computational Chemistry, College of Chemistry, Beijing, China. E-mail: leim@mail.buct.edu.cn*
[b]*Beijing Institute of Fashion Technology, School of Materials Design and Engineering, Beijing, China*

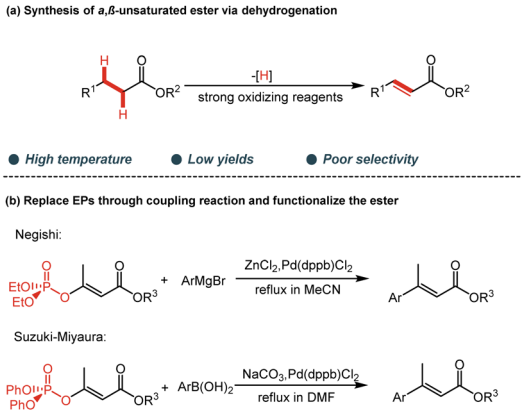

Scheme 2 The synthetic strategies for obtaining α,β-unsaturated esters through (a) direct dehydrogenation and (b) replacing EP and ester functionalization.

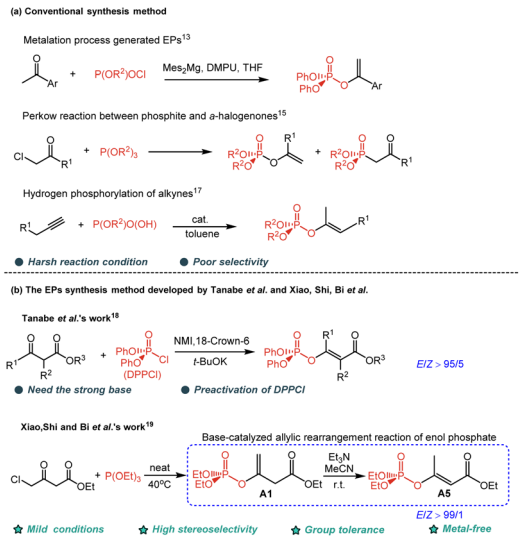

Scheme 3 Synthesis of enol phosphate compounds. (a) Conventional synthesis strategies for enol phosphates (EPs)[13,15,17] (b) synthesis of EPs developed by Tanabe *et al.* and Xiao, Shi, Bi *et al.* (the blue dashed rectangle denotes the NEt3-catalyzed allylic rearrangement reaction of enol phosphate).[18,19]

methods usually require harsh conditions, involve toxic substances, and exhibit limited selectivity.

In 2015, Tanabe *et al.* reported a type of Perkow reaction of α-substituted β-ketoesters and phosphorylating reagent (DPPCl) to synthesize EPs (see Scheme 3b), which could achieve the phosphorylation of α-substituted β-ketoesters assisted by N-methylimidazole (NMI) and *t*-BuOK. However, the pre-activation of diphenyl phosphorochloridate (DPPCl) and the requirement for a strong base limited this reaction.[18] In 2023, Xiao, Shi and Bi *et al.* reported another Perkow reaction of 4-chloroacetoacetates and phosphites to synthesize EPs *via* the base (triethylamine, NEt_3)-catalyzed allylic rearrangement reaction of enol phosphate (see the blue dashed rectangle in Scheme 3b).[19] In this method, 4-chloroacetate reacts with phosphite to produce the β-phosphoroxylated allylic ester, which subsequently undergoes NEt_3-catalyzed allylic rearrangement to produce the corresponding EPs (β-phosphoroxylated α,β-unsaturated ester). This reaction can be carried out smoothly under mild conditions, and the (*E*)-isomer could be produced with excellent stereoselectivity. Interestingly, when NEt_3 was replaced with the stronger base *t*-BuOK or the weaker base pyridine, the reaction did not occur under the same conditions. The base-catalyzed allylic rearrangement reaction of enol phosphate (**A1**) to the final product (**A5**) is of importance for the whole reaction. However, the mechanism for this rearrangement reaction, the origin of the *E*/*Z* stereoselectivity, and the effect of base modulation are still unclear.

In this work, the reaction mechanism of the NEt_3-catalyzed allylic rearrangement reaction of EPs was investigated using density functional theory (DFT) methods. The nature of the *E*/*Z* stereoselectivity is unveiled, and the pivotal role of base and the catalytic effects of bases on the rearrangement are discussed.

Computational methods

All the calculations were performed with the Gaussian 09 program.[20] All geometry optimizations and frequency calculations were performed at the M06-2X/def2-SVP level.[21] The solvent effect of acetonitrile ($\varepsilon = 35.68$) was considered by using the solvation model based on density (SMD).[22] The improved elastic image pair (i-EIP) method was used to assist in finding transition states.[23,24] All stationary points were confirmed by vibrational analysis and characterized by zero imaginary frequencies for intermediates or by only one imaginary frequency for transition states (TSs). Intrinsic reaction coordinates (IRC) calculations were performed in order to confirm intermediates along the reaction pathway.[25] Energy decomposition analysis (EDA) was carried out using the XACS Cloud platform and the Xiamen Energy Decomposition Analysis (XEDA) program.[15,26] Single-point energy calculations were performed at the M06-2X/def2-TZVPP level, using geometries optimized at the M06-2X/def2-SVP level. Unless otherwise noted, all energies discussed in the following sections are Gibbs free energies calculated at 298.15 K. A correction factor of 1.89 kcal mol^{-1} was applied for the standard state transition from 1 atm to 1 M.[27,28] Total energies and Cartesian coordinates of all optimized structures are given in the SI.

Results and discussion

The mechanism of the NEt_3-catalyzed rearrangement of enol phosphate

The experiments reported by Xiao, Shi and Bi *et al.*[19] show that the (*E*)-β-phosphorylated α,β-unsaturated ester **A5** could be obtained in high yield from β-phosphoroxylated allylic ester **A1** *via* two proton-transfer steps catalyzed by NEt_3. The reaction mechanism through which the α,β-unsaturated ester was produced was studied from unconjugated β-phosphate allyl ester **A1**, as shown in Fig. 1. Path A shows the pathway to (*E*)-β-phosphorylated α,β-unsaturated esters **A5**, and Path B shows the pathway to (*Z*)-β-phosphorylated α,β-unsaturated esters **B5**. In Path A, NEt_3

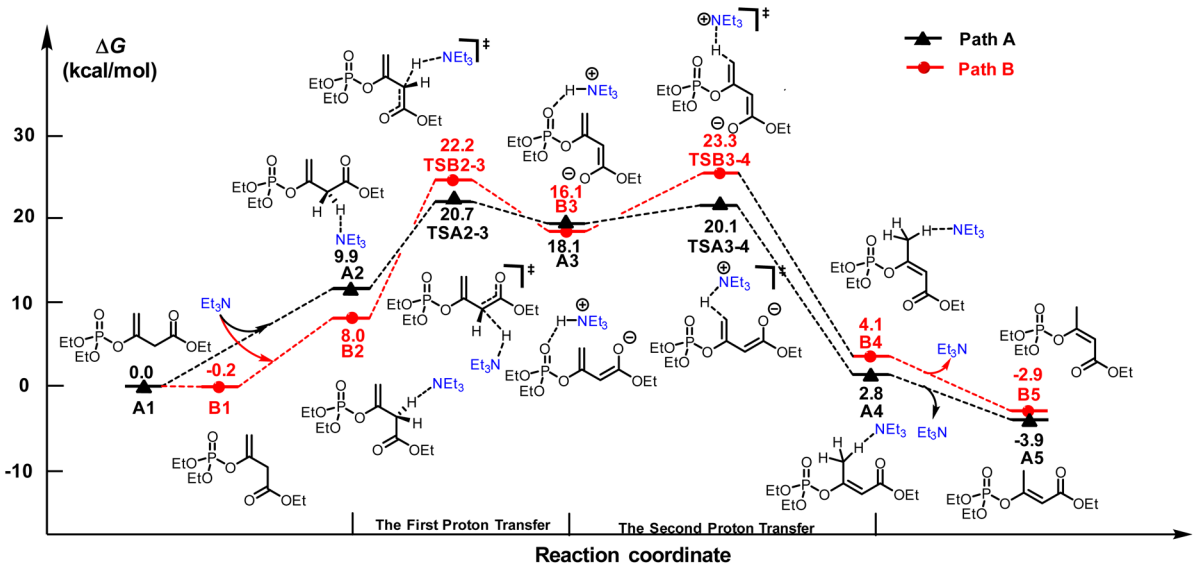

Fig. 1 The Gibbs energy profiles of the mechanism of the allylic rearrangement reaction of enol phosphates catalyzed by NEt_3.

approaches the substrate **A1** to form intermediate **A2**, which is endergonic by 9.9 kcal mol^{-1}. In the first proton-transfer step, the α-H of **A2** is transferred to NEt_3 *via* **TSA2-3** to form **A3** with an energy barrier of 20.7 kcal mol^{-1}. Subsequently, the proton of $HNEt_3^+$ transfers to the γ-C of **A3** *via* **TSA3-4** to form **A4** in the second proton-transfer step. The energy barrier for this step is 2.0 kcal mol^{-1}, with an overall energy barrier of 20.7 kcal mol^{-1}. Finally, the whole reaction is completed with the release of NEt_3 and the generation of the product **A5**. The reaction mechanism along Path B is very similar to that along path A. Firstly, **A1** could directly isomerize to **B1** through rotation of the C–C bond. Then NEt_3 approaches the substrate **B1** to form intermediate **B2**, which is endergonic by 8.2 kcal mol^{-1}. In the first proton-transfer step, the α-H of **B2** is transferred to NEt_3 to form **B3**, with an energy barrier of 22.2 kcal mol^{-1} *via* **TSB2-3**. Then, in the second proton-transfer step, the proton of the $HNEt_3^+$ moiety of **B3** transfers to the γ-C *via* **TSB3-4** to form **B4**. The energy barrier for this step is 7.0 kcal mol^{-1}, with an overall energy barrier of 23.3 kcal mol^{-1}. Finally, the whole reaction is completed with the release of NEt_3 and the generation of the product **B5**. The calculated results show that the rate-determining step is the first proton-transfer step with energy barriers of 20.7 kcal mol^{-1} and 23.3 kcal mol^{-1} for Paths A and B, respectively. Path A is favoured and the (*E*)-β-phosphorylated α,β-unsaturated ester **A5** is formed as the dominant product, which is consistent with the experiments.[19] Other possible reaction pathways can be found in SI (Fig. S2).

The origin of the *Z*/*E* stereoselectivity

The calculated results showed that the first proton-transfer step is the rate- and selectivity-determining step. To gain a deeper insight and reveal the nature of the *E*/*Z* stereoselectivity, generalized Kohn–Sham energy decomposition analysis (GKS-EDA) was performed.[29] GKS-EDA divides the total interaction energy (ΔE^{tot}) into electrostatic (ΔE^{elec}), exchange-repulsion ($\Delta E^{ex\text{-}rep}$), polarization (ΔE^{pol}), correlation (ΔE^{corr}), and dispersion (ΔE^{disp}) terms.[30,31] The electrostatic term (ΔE^{elec}) is the Coulomb interaction energy between the fragments with frozen orbitals; this includes both the attractive and repulsive interactions between the two fragments. The exchange-repulsion term ($\Delta E^{ex\text{-}rep}$) is associated with Pauli repulsion, representing an unfavorable repulsive component as a result of the overlapping electron densities of the interacting groups, and is reflective of steric interaction. The polarization term (ΔE^{pol}) is associated with orbital interaction. The correlation term (ΔE^{corr}) is the contribution of the correlation energy, reflecting instantaneous electron–electron interactions that further stabilize the complex.[32] It is notable that the Grimme dispersion correction (ΔE^{disp}) term is constantly 0 kcal mol^{-1}, which means that the dispersion contribution is included in the electron correlation energy (ΔE^{corr}) rather than having no dispersion effect.

As shown in Fig. 2a, the key transition state structures (**TSA2-3** and **TSB2-3**) were divided into two parts: unconjugated β-phosphate allyl ester (fragment 1) and NEt_3 (fragment 2). The EDA showed that the higher (more negative) exchange energy (ΔE^{ex}) and higher electrostatic energy (ΔE^{elec}) in **TSA2-3** are major contributing factors leading to the adoption of the *E* conformation. In **TSA2-3**, the C–H on the NEt_3 ethyl group faces a phosphoester oxygen, which can form a moderate-intensity C–H···O contact, providing additional electrostatic attraction and polarization stability. In **TSB2-3**, such C–H···O contacts are dispersed or elongated, and thus cannot exert the same stabilizing effect. In **TSA2-3**, the attractive interactions from the electrostatic, exchange, and polarization terms are all stronger than in **TSB2-3**. Although the repulsive energy of **TSA2-3** is larger than that of **TSB2-3**, the values of ΔE^{tot} suggest that **TSA2-3** has stronger intermolecular interactions than **TSB2-3**. In general, the *E* configuration of **TSA2-3** has a tighter charge distribution and better electrostatic and orbital (exchange, polarization) interaction, which makes **TSA2-3** more stable than **TSB2-3**. Moreover, in **TSB2-3**, two non-bonded phosphate oxygens

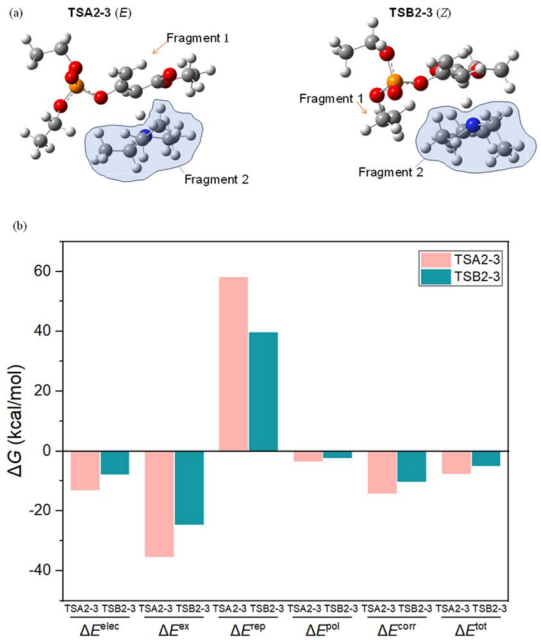

Fig. 2 (a) Geometric structures of **TSA2-3** and **TSB2-3**. (b) EDA for **TSA2-3** and **TSB2-3** calculated at the M06-2X/def2-SVP level of theory.

approach each other more closely, creating a compact folded geometry, while significantly amplifying lone-pair-lone-pair repulsion. This enhanced steric clash raises the exchange-repulsion component and simultaneously hinders the formation of certain C–H···O attractions that are seen in **TSA2-3.**

Origin of deactivation of the rearrangement by pyridine and *t*-BuOK base catalysts

The experimental results[19] show that different bases have a significant impact on the reaction. Neither the stronger base *t*-BuOK nor the weaker base pyridine catalyzes the reaction effectively. The mechanism of the allylic rearrangement reaction catalyzed by *t*-BuOK and pyridine was also investigated. As shown in Fig. 3, Path C represents the reaction mechanism catalyzed by pyridine, and Path D represents the reaction mechanism catalyzed by *t*-BuOK. In Path C, the pyridine approaches the substrate **C1** and interacts with the α-H moiety through hydrogen bonding to form intermediate **C2**, which is endergonic by 8.0 kcal mol^{-1}. In the first proton-transfer step, the α-H of **C2** is transferred to pyridine *via* **TSC2-3** to form **C3**; the energy barrier for this step is 26.1 kcal mol^{-1}. In the second proton-transfer step, the proton of protonated pyridine transfers to the γ-C of **C3** *via* **TSC3-4** to form **C4**, with an energy barrier of 4.5 kcal mol^{-1} and an overall energy barrier of 26.5 kcal mol^{-1}. Finally, **A5** is formed with the release of pyridine from **C4**. In Path D, the α-H of **D2** is transferred to the O atom of *t*-BuOK to form a stable intermediate **D3** *via* **TSD2-3** with an energy barrier of 3.4 kcal mol^{-1}, which is exergonic by 20.8 kcal mol^{-1}. Then the hydrogen atom of *t*-BuOH is transferred to the γ-C of **D3** *via* **TSD3-4** to form **D4** with an energy barrier of 27.7 kcal mol^{-1}. Finally, the whole reaction is completed with the release of the base and the generation of the product **A5**. The calculated results show that neither a strong base (*t*-BuOK) nor a weak base (pyridine) can effectively catalyze the reaction. While it is difficult for weak bases such as pyridine to accept a proton from the substrate during the first proton-

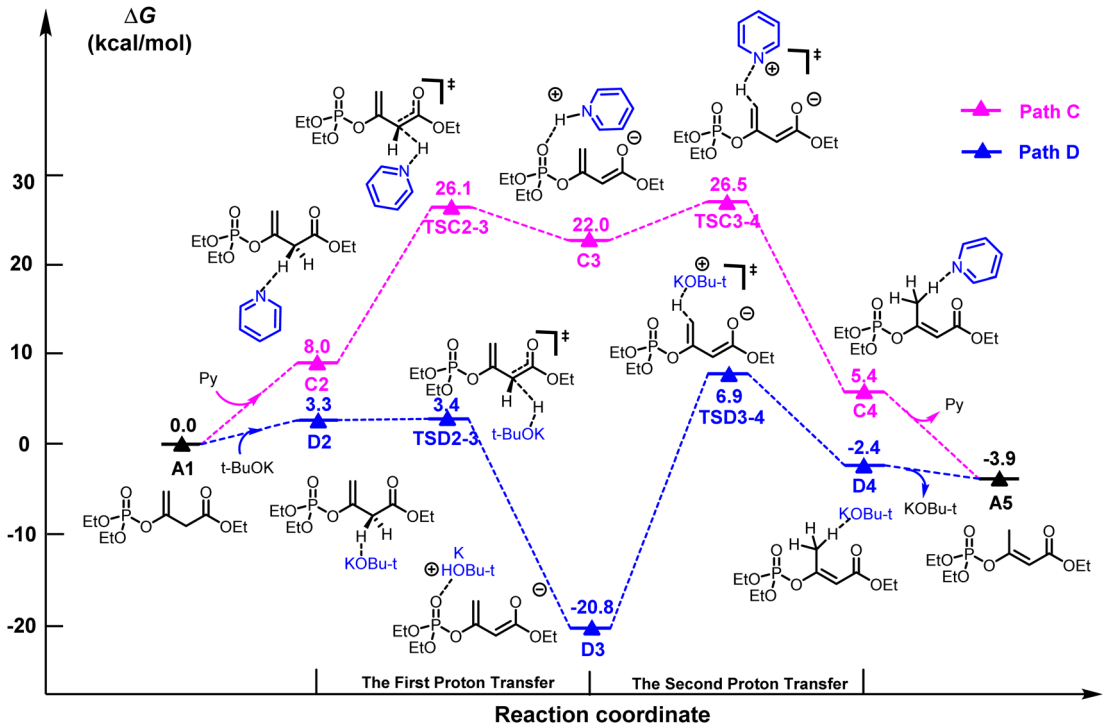

Fig. 3 Gibbs energy profiles of the mechanism of the allylic rearrangement reaction of enol phosphates catalyzed by *t*-BuOK and pyridine.

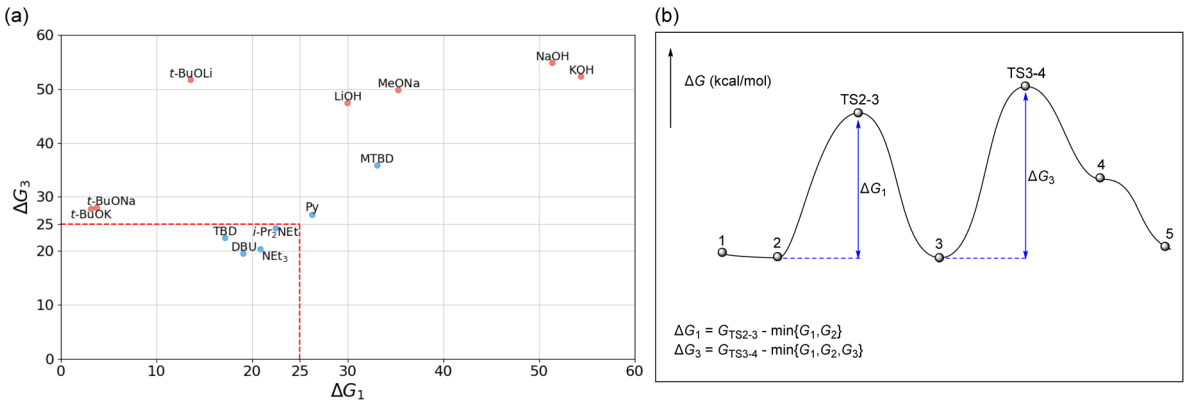

Fig. 4 (a) The two-dimensional energy barrier map of ΔG_1 and ΔG_3. (b) Schematic of the barrier definitions along the reaction coordinate.

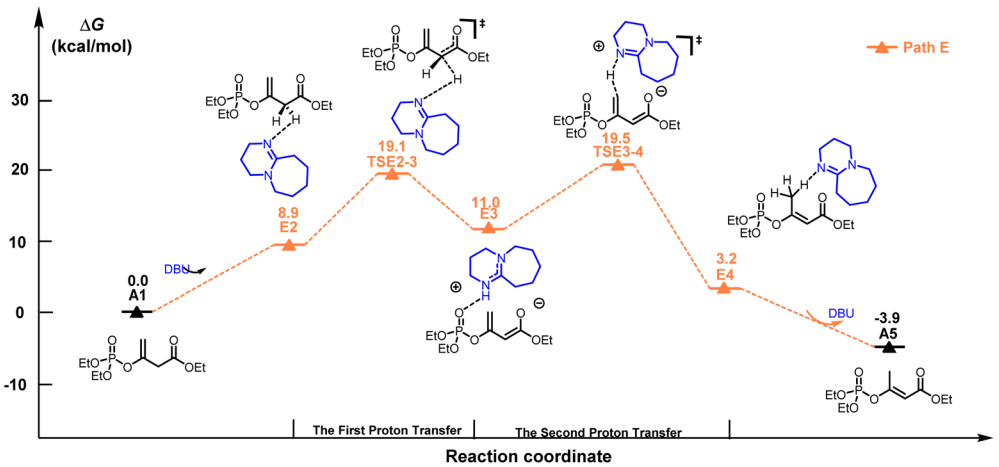

Fig. 5 Gibbs energy profiles of the mechanism of the allylic rearrangement reaction of enol phosphates catalyzed by DBU.

transfer step, strong bases, such as *t*-BuOK, do not perform well in the second proton-transfer step due to the stability of intermediate **D3**.

The modulation effect of bases on the rearrangement

Our calculated results revealed that the nature of the base can significantly influence the reactions. To find a more efficient catalyst for the rearrangement reaction of β-phosphoroxylated allylic esters, a series of bases was selected to investigate the reaction.[33] As shown in Fig. 4, the energy barriers to reach the transition states in the rearrangement reaction of the β-phosphoroxylated allylic ester catalyzed by thirteen bases (organic bases are shown in blue and inorganic bases are shown in red) were calculated and a two-dimensional energy barrier map of ΔG_1 (the first proton transfer energy barrier) and ΔG_3 (the second proton transfer energy barrier) was constructed (see details of the calculated results in the SI). By applying dual thresholds ($\Delta G_1 < 25$ kcal mol^{-1} and $\Delta G_3 < 25$ kcal mol^{-1}), some organic bases (NEt_3, DBU, TBD and *i*-Pr_2NEt) were determined to have good catalytic activity, and all inorganic bases exhibited inferior catalytic activity (see Fig. 4). The calculated results show that DBU could act as a catalytic species in this rearrangement reaction with the highest catalytic activity. The catalytic effect of DBU is also excellent, being superior to those of NEt_3 and (*i*-Pr)$_2$NEt. On the contrary, when MTBD was used as the catalyst, an energy barrier of 35.8 kcal mol^{-1} was calculated for the reaction. Therefore, MTBD and pyridine do not catalyze the reaction well. Fig. 5 shows the Gibbs energy profile of the allylic rearrangement reaction catalyzed by DBU. The energy barrier is 19.1 kcal mol^{-1} and 8.5 kcal mol^{-1} for the first and second proton-transfer steps, respectively, with a global barrier of 19.5 kcal mol^{-1}. It has been reported that the solubility of strong base reagents (*e.g.*, NaOH, *t*-BuOK) in the reaction medium may have an impact on the reaction energy barrier.[34] Our model ignores the solubility effect of strong bases. Nevertheless, the calculated results successfully reproduce the experimental selectivity trend using this simple model.

Conclusions

In conclusion, we performed a detailed theoretical study of the mechanism of the NEt_3-catalyzed allylic rearrangement reaction of enol phosphates using DFT method. The calculations show that the rearrangement reaction proceeds through two proton-

transfer steps to generate the product with *E* configuration. The rate-determining step is the first proton-transfer step for the reaction of the NEt_3-catalyzed allylic rearrangement of enol phosphates, with an energy barrier of 20.7 kcal mol^{-1}. The weak base, pyridine, is not able to effectively accept proton from the substrate during the first proton-transfer step, and the strong base, *t*-BuOK, does not perform well in the second proton-transfer step, which requires a proton from the catalytic species. Additionally, the results suggest the possibility of substituting other bases for the reaction and provide a mechanistic explanation for the reactivity of the bases discussed in the experiment. DBU exhibits the best performance among these bases; the rate-determining step is the first proton-transfer step, with an energy barrier of 19.1 kcal mol^{-1}. This study could provide valuable guidance for developing advanced methodologies in synthetic organic chemistry, with potential applications in pharmaceutical development, materials science, and sustainable chemical steps.

Author contributions

The manuscript was written through contributions of all authors. All authors have given approval to the final version of the manuscript.

Conflicts of interest

There are no conflicts to declare.

Data availability

The data supporting this article have been included as part of the SI. Supplementary information is available. See DOI: **https://doi.org/10.1039/d5ra05485k**.

Acknowledgements

This work was supported by the National Natural Science Foundation of China (Grant No. 22473008, 22411530047) and the Beijing Municipal Natural Science Foundation (Grant No. 2242014). We also thank the High Performance Computing (HPC) Platform at Beijing University of Chemical Technology (BUCT) for providing part of the computational resources.

References

1 S. Gnaim, J. C. Vantourout, F. Serpier, P.-G. Echeverria and P. S. Baran, *ACS Catal.*, 2021, **11**, 883–892.
2 Y. Xu, R. Zhang, B. Zhou and G. Dong, *J. Am. Chem. Soc.*, 2024, **146**, 22899–22905.
3 H. Chen, L. Liu, T. Huang, J. Chen and T. Chen, *Adv. Synth. Catal.*, 2020, **362**, 3332–3346.
4 J. Muzart, *Eur. J. Org Chem.*, 2010, **2010**, 3779–3790.
5 X. Zhang, M. Chang, T. Ni, X. Zhang, Q. Zhao, W. Li and T. Li, *Org. Lett.*, 2024, **26**, 6619–6624.
6 A. B. Flynn and W. W. Ogilvie, *Chem. Rev.*, 2007, **107**, 4698–4745.
7 Y. Ashida and Y. Tanabe, *Chem. Rec.*, 2020, **20**, 1410–1429.
8 M. Shindo, Y. Sato, T. Yoshikawa, R. Koretsune and K. Shishido, *J. Org. Chem.*, 2004, **69**, 3912–3916.
9 A. B. Lemay, K. S. Vulic and W. W. Ogilvie, *J. Org. Chem.*, 2006, **71**, 3615–3618.
10 Y. Yamamoto, N. Kirai and Y. Harada, *Chem. Commun.*, 2008, 2010–2012.
11 J. D. Sellars and P. G. Steel, *Chem. Soc. Rev.*, 2011, **40**, 5170–5180.
12 P. Zhang, Z. Li, Y. Liu, F. Shi, L. Wang, M. Pu and M. Lei, *J. Org. Chem.*, 2022, **87**, 12997–13010.
13 W. J. Kerr, D. M. Lindsay, V. K. Patel and M. Rajamanickam, *Org. Biomol. Chem.*, 2015, **13**, 10131–10135.
14 Y. Cao, Z. Gao, J. Li, X. Bi, L. Yuan, C. Pei, Y. Guo and E. Shi, *RSC Adv.*, 2020, **10**, 29493–29497.
15 B. G. Janesko, *J. Phys. Chem. Lett.*, 2022, **13**, 5698–5702.
16 A. Inial, F. Morlet-Savary, J. Lalevée, A. C. Gaumont and S. Lakhdar, *Org. Lett.*, 2020, **22**, 4404–4407.
17 P. H. Lee, S. Kim, A. Park, B. C. Chary and S. Kim, *Angew. Chem., Int. Ed.*, 2010, **122**, 6958–6961.
18 H. Nakatsuji, Y. Ashida, H. Hori, Y. Sato, A. Honda, M. Taira and Y. Tanabe, *Org. Biomol. Chem.*, 2015, **13**, 8205–8210.
19 Y. Zhang, H. Guo, Q. Wu, X. Bi, E. Shi and J. Xiao, *RSC Adv.*, 2023, **13**, 13511–13515.
20 R. A. Gaussian 09, M. J. Frisch, G. W. Trucks, H. B. Schlegel, G. E. Scuseria, M. A. Robb, J. R. Cheeseman, G. Scalmani, V. Barone, G. A. Petersson, H. Nakatsuji, X. Li, M. Caricato, A. Marenich, J. Bloino, B. G. Janesko, R. Gomperts, B. Mennucci, H. P. Hratchian, J. V. Ortiz, A. F. Izmaylov, J. L. Sonnenberg, D. Williams-Young, F. Ding, F. Lipparini, F. Egidi, J. Goings, B. Peng, A. Petrone, T. Henderson, D. Ranasinghe, V. G. Zakrzewski, J. Gao, N. Rega, G. Zheng, W. Liang, M. Hada, M. Ehara, K. Toyota, R. Fukuda, J. Hasegawa, M. Ishida, T. Nakajima, Y. Honda, O. Kitao, H. Nakai, T. Vreven, K. Throssell, J. A. Montgomery, Jr., J. E. Peralta, F. Ogliaro, M. Bearpark, J. J. Heyd, E. Brothers, K. N. Kudin, V. N. Staroverov, T. Keith, R. Kobayashi, J. Normand, K. Raghavachari, A. Rendell, J. C. Burant, S. S. Iyengar, J. Tomasi, M. Cossi, J. M. Millam, M. Klene, C. Adamo, R. Cammi, J. W. Ochterski, R. L. Martin, K. Morokuma, O. Farkas, J. B. Foresman, and D. J. Fox, *Gaussian 09 Rev. B. 01*, Wallingford, CT, 2009.
21 Y. Zhao and D. G. Truhlar, *Theor. Chem. Acc.*, 2008, **120**, 215–241.
22 A. V. Marenich, C. J. Cramer and D. G. Truhlar, *J. Phys. Chem. B*, 2009, **113**, 6378–6396.
23 Y. Liu, H. Qi and M. Lei, *J. Chem. Theory Comput.*, 2022, **18**, 5108–5115.
24 Y. Liu, H. Qi and M. Lei, *J. Chem. Theory Comput.*, 2023, **19**, 2410–2417.
25 H. P. Hratchian and H. B. Schlegel, *J. Chem. Phys.*, 2004, **120**, 9918–9924.
26 L. Song, W. Wu, Q. Zhang and S. Shaik, *J. Comput. Chem.*, 2004, **25**, 472–478.
27 V. S. Bryantsev, M. S. Diallo and W. A. Goddard, 3rd, *J. Phys. Chem. B*, 2008, **112**, 9709–9719.

28 D. Huang, O. V. Makhlynets, L. L. Tan, S. C. Lee, E. V. Rybak-Akimova and R. H. Holm, *Proc. Natl. Acad. Sci. U.S.A.*, 2011, **108**, 1222–1227.
29 Z. Tang, Y. Song, S. Zhang, W. Wang, Y. Xu, D. Wu, W. Wu and P. Su, *J. Comput. Chem.*, 2021, **42**, 2341–2351.
30 M. W. Schmidt, K. K. Baldridge, J. A. Boatz, S. T. Elbert, M. S. Gordon, J. H. Jensen, S. Koseki, N. Matsunaga, K. A. Nguyen, S. Su, T. L. Windus, M. Dupuis and J. A. Montgomery Jr, *J. Comput. Chem.*, 1993, **14**, 1347–1363.
31 P. Su, Z. Jiang, Z. Chen and W. Wu, *J. Phys. Chem. A*, 2014, **118**, 2531–2542.
32 A. Thayyil and P. C. Parambil, *ChemPhysChem*, 2023, **24**, e202200761.
33 L. Zhang, B. Wang, Y. Zhao, M. Pu, S. Liu and M. Lei, *J. Phys. Chem.*, 2021, **125**, 2316–2323.
34 J. R. Pliego, *J. Mol. Liq.*, 2017, **237**, 157–163.